

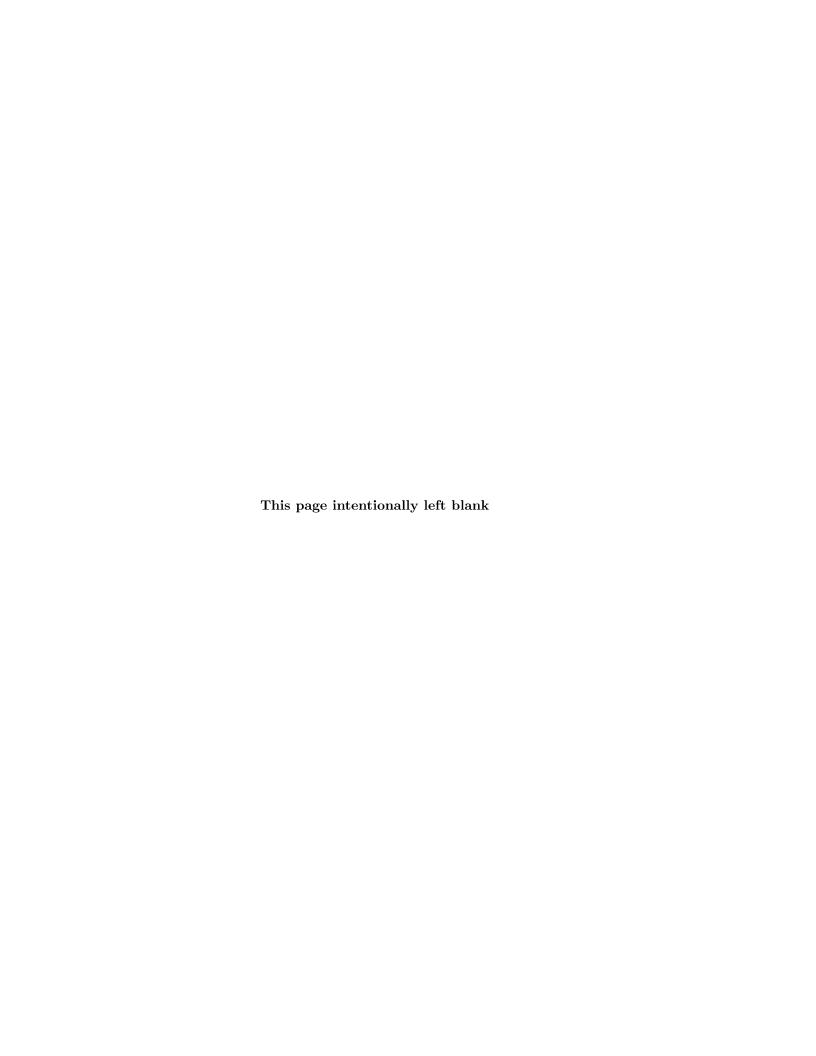
Department of Civil, Environmental and Architectural Engineering University of Genoa

NUMERICAL SIMULATION OF THE UNSTEADY AERODYNAMICS OF FLAPPING FLIGHT

Joel GUERRERO

A thesis submitted for the degree of $Doctor\ of\ Philosophy$

April 2009



Contents

1	Intr	roduction	1
	1.1	Overview	1
	1.2	Objectives	4
	1.3	Outline of the dissertation	5
2	Aer	odynamics of Flapping Flight	7
	2.1	Flight in Nature	7
		2.1.1 Unpowered Flight: Gliding and Soaring	8
		2.1.2 Powered Flight: Flapping	10
		2.1.3 Hovering	12
		2.1.4 Take-off and landing	13
		2.1.5 Summary	15
	2.2	Brief History of Flapping Wing Research: Experimentation, Observations, Ana-	
		lytical and Computational Approaches	15
	2.3	The Physics of Drag and Thrust Generation Due to Wing Flapping	21
	2.4	The Phenomenon of Dynamic Stall and Leading Edge Vortex (LEV) Shedding	24
	2.5	Reynolds Number in Terms of Flapping Flight	25
	2.6	Strouhal Number and Reduced Frequency	26
		2.6.1 Strouhal Number as the Fundamental Aerodynamic Parameter in Flapping	
		Flight	27
	2.7	Flapping Airfoils Performance Parameters	28
	2.8	Airfoil Geometry and Flapping Kinematics	30
3	Gov	verning Equations of Fluid Dynamics	34
	3.1	Navier-Stokes System of Equations	34
	3.2	Nondimensionalization of the Governing Equations	37
	3.3	9 1	41
	3.4	Simplification of the Navier-Stokes System of Equations: Incompressible Viscous	
		Flow Case	47
4	On	Structured Overlapping Grids	52
	4.1	Approaches to Grid Generation	52
	4.2	Overview and Historical Background of the Structured Overlapping Grids Method	57
	4.3	Problem Formulation	61
	-	4.3.1 Extension of the Overlapping Grids Method to Moving Boundaries Problems	
		4.3.2 Time Stepping Algorithm	68
	4.4	Overlapping Grids Assembling Algorithm	69
	4.5	Discretization on Overlapping Grids	73

	4.6	Comments on Overlapping Grids
5	Nu	merical Method 70
	5.1	Primitive Variable Formulation of the Incompressible Navier-Stokes Equations 79
	5.2	Pressure-Poisson Equation (PPE) or Velocity-Pressure Formulation in Primitive
		Variables
	5.3	Remarks on the Pressure Boundary Condition
	5.4	Spatial Discretization of the Velocity-Pressure Formulation of the Incompressible
		Navier-Stokes Equations
	5.5	Time-Stepping Algorithm for the Velocity-Pressure Formulation of the Incompress-
		ible Navier-Stokes Equations
	5.6	Velocity-Pressure Formulation for Moving Overlapping Grids
		5.6.1 Boundary Conditions for Moving Walls
	5.7	Boundary Conditions
	5.8	Discrete Divergence Damping
6	Val	idation and Verification of the Navier-Stokes Flow Solver 89
	6.1	Flow Solver Validation and Verification. General Issues
	6.2	Numerical Results and V&V
		6.2.1 The Method of Manufactured Solutions or Forced Solutions 9
		6.2.2 Flow Past a Stationary Cylinder at Various Reynolds Number Values 9
		6.2.3 Comparison of Fixed Body Solution vs. Moving Body Solution 10
		6.2.4 Comparison to other Numerical and Experimental Results
		6.2.5 Comparison of Sequential Vs. Parallel Computations
	6.3	Grid Refinement Study
		6.3.1 Quantitative Study - Force Measurements
		6.3.2 Qualitative Validation - Wake Structures Resolution
		6.3.3 Summary of the Quantitative and Qualitative Grid Refinement Study 12
	6.4	Closing Remarks
7	Wa	ke Structures and Aerodynamic Performance of Flapping Airfoils 12'
	7.1	Introduction
	7.2	Heaving Airfoil Wake Signature and Aerodynamic Performance
	7.3	Leading Edge Vortex Shedding and Frequency Dependence
	7.4	Flapping airfoils (Coupled Heaving-and-Pitching Motion)
		7.4.1 Effect of Maximum Pitching Angle
		7.4.2 Effect of Heaving Amplitude
		7.4.3 Effect of Strouhal Number
		7.4.4 Effect of Phase Angle
		7.4.5 Propulsive Efficiency, Thrust Coefficient and Input Power Coefficient Con-
		tour Maps
	7.5	Heaving Airfoil Vs. Flapping Airfoil
	7.6	Effect of Flexibility on the Aerodynamic Performance
	7.7	Effect of Airfoil Cambering on the Aerodynamic Performance
	7.8	Summary 16

8	Wal	ke Topology and Aerodynamic Performance of Finite-Span Flapping Wings	172
	8.1	Overview	172
	8.2	Computational Domain and Grid Setup	172
	8.3	Vortex Identification	174
	8.4	Heaving Wing	
	8.5	Flapping Wing	183
	8.6	Aspect Ratio Influence on the Aerodynamics Performance	189
	8.7	Rolling Wing	192
	8.8	Summary	
9	Cor	aclusions and Perspectives	201
	9.1	Conclusions	201
		Perspectives for future work	
\mathbf{A}	Con	npanion DVD with selected animations	206
Bi	bliog	graphy	208

List of Figures

1.1	Published ranges (taken from [182]) of St for cruising birds, bats, fishes, sharks and dolphins. Dotted lines mark the range $0.2 < St < 0.4$, in which propulsive efficiency usually peaks; dashed line marks the modal peak at $St = 0.3$. Unbroken lines indicate the range of variation in St across other non-zero flight speeds, where such data exist	3
2.1	A bird while gliding. Notice the separation between the wingtip feathers; these natural slots, help to reduce the induced drag while gliding	8
2.2	In gliding flight, a bird's wing deflect air downward, causing a lift force that holds the bird up in the air (see figure A). By tilting forward and going into a slight dive	
2.3	(figure B), the bird can maintain forward speed	9
	maintain or gain altitude and save energy	9
2.4	A Mallard in powered flight (flapping flight)	10
2.5	In A, the wings twist as shown to maintain the correct angle of attack for the downstroke. In B, the bird's wings produce lift and thrust during the downstroke.	11
2.6	In A, the inner part of the wing produces lift, even during the upstroke. In B, the outer part of the wing is angled to pass through the air with little resistance	11
2.7	Wingtip paths relative to the body for two natural flyers. (A) Pigeon (Columba Livia), here we see the path transition from tip-reversal upstrokes during slow flight to feathered upstrokes at intermediate speeds and a swept-wing upstroke during fast flight. (B) Black-billed magpie (Pica Hudsonica) wingtip path at all flight speeds [187]	12
2.8	Hovering flight: a) asymmetric hovering or "avian stroke" and b) symmetric hovering or "insect stroke"	13
2.9	Illustration of a hummingbird in hovering flight. In the bottom figure, humming-	10
2.0	bird 's wing figure-eight pattern is shown	14
2.10	A bufflehead running atop the water while taking off	14
	Precision touchdown of an eastern imperial eagle on a tree branch	15
	Thrust (T) and lift (L) components of the normal force vector (N) during heaving	
	motion	16
2.13	Dye visualizations of different wakes behind an oscillating airfoil (from von Karman vortex street, to neutral wake, to reverse von Karman vortex street, to deflected	
	wake)	18
2.14	Vortex street indicative of drag production (drag producing wake) [93]	21
	Vortex street indicative of thrust production (thrust producing wake) [93]	22
2.16	Vortex street indicative of zero drag (neutral wake) [93]	23

2.17	Dual-mode or nonsymmetric vortex street indicative of thrust and lift production (deflected wake) [93]	23
2.18	Dynamic stall on a heaving airfoil during downstroke (sequence is top-to-bottom left column, then top-to-bottom right column)	25
2.19	Airfoil geometry and airfoil motion. In the figure, heaving motion $y(t)$ of the pivot point, pitching motion $\alpha(t)$ of the airfoil about the pivot point, maximum heaving amplitude h_a , maximum pitching amplitude α_a , airfoil chord c, pivot point x_p and	
	free-stream velocity U_{∞} are shown	30
	Different possible combination of motions and effect of phase angle in $2\mathbb{D}$	32
	$3\mathbb{D}$ flapping wing kinematics	33
2.22	Positional, elevation and feathering angle variations for one period for a hovering hawkmoth [167]	33
3.1	Correspondence between the physical space (Cartesian coordinates) and the computational space (generalized curvilinear coordinates)	42
3.2	Transformation from physical space to computational space. Left: structured grid in physical space. Right: logically uniform grid in computational space	43
4.1	Single-block C-type structured grid around a NACA 4412 airfoil	53
4.2	Multi-block structured grid around a NLR 7301 airfoil with flap	54
4.3	Overlapping structured grid around a NLR 7301 airfoil with flap	55
4.4	Unstructured mesh around a NHLP-2D three element airfoil	56
4.5	Cartesian grid around a Drela DAE11 low Reynolds number airfoil	57
4.6	Simple overlapping grid system in physical space \mathcal{P}	59
4.7	Simple overlapping grid system consisting of two component grids \mathcal{G}_g . An annular boundary fitted grid (\mathcal{G}_2) and a background Cartesian grid (\mathcal{G}_1) . The top view shows the overlapping grid in physical space \mathcal{P} while the bottom view shows each grid in computational space \mathcal{C}	63
4.8	Interpolation scheme for overlapping grids. The interpolation is performed in com-	
	putational space C	65
4.9 4.10	Explicit and implicit interpolation for a one-dimensional overlapping grid Moving overlapping grid. The new overlapping grid system \mathbb{G} interpolation stencils	66
1.10	and chimera holes are determined by Ogen at each time step	67
4.11	Pseudo C++ Code for the basic time stepping algorithm for overlapping grids	69
	Left. Initial overlapping grids system \mathbb{G} . Right. Individual component grids \mathcal{G}_q .	70
	Overlapping grid system \mathbb{G} after cutting holes and removing all exterior or unused points. The hole cutting algorithm generates a barrier of unused points and	
	interpolation points that bounds the entire hole region	71
4.14	Overlapping grid system \mathbb{G} after marking points on the physical boundaries (stairstep boundary) and interpolation boundaries	71
4.15	Overlapping grid system $\mathbb G$ after marking all proper interpolation	72
4.16	Final overlapping grid system $\mathbb G$ after removing excess of interpolation points $\ . \ .$	73
4.17	Overlapping grid discretization in one dimension	74
5.1	General boundary configuration for external flows	86

6.1	Forced solutions of the incompressible Navier-Stokes equations around a circle in a square with slip wall boundaries and $\omega_0 = \omega_1 = \omega_3 = 1$. Top-to-bottom left column, grid system from coarser grid to finer grid. Top-to-bottom right column, corresponding grid level velocity u contours. Notice how the quality of the solution improves as the grid is refined	. 92
6.2	Domain and overlapping grid system of the unsteady flow past a cylinder case. Top view: overall domain. Bottom view: close-up of the grid around the cylinder.	. 93
6.3	Streamlines for $Re = 20$ (top figure) and $Re = 40$ (bottom figure) for a nondimensional time $t = 400$. 94
6.4	Vorticity contours for $Re = 100$ and $Re = 200$ for a nondimensional time $t = 500$.	. 96
6.5	Time dependent lift and drag coefficient for $Re = 100.$. 98
6.6	Von Karman street onset (stopping criteria for solver benchmarking)	. 100
6.7	Left: computational domain for the fixed cylinder case. Right: computational domain for the moving cylinder case (the cylinder is in the initial position and it	100
C O	moves from right to left).	. 102
6.8	Moving cylinder vs. fixed cylinder, pressure coefficient c_p comparison at a nondimensional time $t = 7.0. \dots \dots \dots \dots \dots \dots$	102
6.9	Comparison of average thrust coefficient $\overline{c_t}$ results for the pitching airfoil case	. 103
0.9	(negative values indicate drag production)	. 104
6.10		
0.20	(negative values indicate drag production)	. 106
6.11	Comparison of vorticity contours for the heaving-and-pitching airfoil case (case F1 in table 6.10). Left column: vorticity contours obtained by Pedro <i>et al.</i> [140]. Right column: present results. The first row is the beginning of one period, the second row is 1/8 of the period, the third row is 1/4 of the period and the last row is 3/8 of the period	
6.12	Comparison of vorticity contours for the heaving-and-pitching airfoil case (case F6 in table 6.10). Left column: vorticity contours obtained by Pedro <i>et al.</i> [140]. Right column: present results. The first row is the beginning of one period, the second row is 1/8 of the period, the third row is 1/4 of the period and the last row	
	is 3/8 of the period	. 108
	Comparison of variation of thrust coefficient with reduced frequency (negative values indicate drag production)	. 109
	Comparison of vorticity contours between the serial case and the parallel case for a nondimensional time $t=100$. In the figure, NP stands for number of processors.	
	Parallel speed up	. 112
6.16	Top: instantaneous drag coefficient c_d (negative values indicate thrust generation). Bottom: instantaneous lift coefficient c_l . Both quantities are shown for an interval equal to $6 < t < 7$. 116
6.17	Plot of observed quantity values (average thrust coefficient $\overline{c_t}$) for each grid. The equivalent zero grid spacing value is also plotted	. 117
6.18	Instantaneous drag coefficient c_d iterative convergence comparison for the heaving airfoil benchmarking case (negative values indicate thrust production)	. 118
6.19	Grid refinement study of the wake structures resolution for the heaving airfoil benchmarking case. Vorticity contours corresponding to \mathbb{G}_5 (see table 6.19) are	
	shown	. 120

6.20	Grid refinement study of the wake structures resolution for the heaving airfoil benchmarking case. Vorticity contours corresponding to \mathbb{G}_4 (see table 6.19) are shown.	122
6.21	Grid refinement study of the wake structures resolution for the heaving airfoil benchmarking case. Vorticity contours corresponding to \mathbb{G}_3 (see table 6.19) are	122
6.22	Shown	
6.23	Grid refinement study of the wake structures resolution for the heaving airfoil benchmarking case. Vorticity contours corresponding to \mathbb{G}_1 (see table 6.19) are	194
6.24	shown	
7.1	Left: wake structure behind a heaving NACA 0012 airfoil (vorticity contours). Right: horizontal velocity profile measured at a distance equal to 5 times the airfoil chord away from the trailing edge. Flapping parameters: $St = 0.1, h_a = 0.000$	100
7.2	$0.05, Re = 1100$. This configuration is indicative of drag production Left: wake structure behind a heaving NACA 0012 airfoil (vorticity contours). Right: horizontal velocity profile measured at a distance equal to 5 times the airfoil chord away from the trailing edge. Flapping parameters: $St = 0.3, h_a = 0.00$	
7.3	0.15, $Re = 1100$. This configuration is indicative of thrust production Left: wake structure behind a heaving NACA 0012 airfoil (vorticity contours). Right: horizontal velocity profile measured at a distance equal to 5 times the airfoil chord away from the trailing edge. Flapping parameters: $St = 0.15, h_a = 0.25, Re = 1100$. This configuration is indicative of a net balance between thrust production and drag generation (neutral wake)	
7.4	Top figure: time dependent drag and lift coefficients (where negative values of drag coefficient indicate thrust production). Bottom figure: heaving kinematics.	
7.5	Flapping parameters: $Re = 1100, St = 0.4, h_a = 0.2$ ($\overline{c_t} = 0.8834, \overline{c_l} = 0.0098$) Variation of thrust coefficient and propulsive efficiency with the Strouhal number. Flapping parameters: $Re = 1100, f_h = 1$. Notice that the propulsive efficiency is only shown for positive thrust	
7.6	Variation of thrust coefficient and propulsive efficiency with the Strouhal number. Flapping parameters: $Re = 1100, f_h = 0.5$. Notice that the propulsive efficiency is	
7.7	only shown for positive thrust	131
7.8	Flapping parameters: $Re = 1100, St = 0.3$ Variation of thrust coefficient and propulsive efficiency with heaving amplitude.	132
	Flapping parameters: $Re = 1100, St = 0.4$	132
7.9	Plot showing the wake structure classification. Lines of constant Strouhal number value are included to demonstrate the approximate dependence of the wake	199
7.10	topology on the Strouhal number	
	Flapping parameters for both cases: $Re = 1100$, $St = 0.5$, $h_a = 0.3$	
7.11	Horizontal velocity profile evolution as function of the Strouhal number	134

7.12	Time dependent lift coefficient for two different heaving cases. Notice that for the case $St = 0.5 (h = 0.3)$, the lift coefficient evolution is not symmetric about the horizontal mean line, this is due to the angle of attack induced by the deflected wake, the bumps on the lift curve are due to the dynamic stall ($\overline{c_l} = 0.10923$). For the case $St = 0.3 (h = 0.15)$ the lift evolution is symmetrical about the horizontal
	mean line $(\overline{c_l} = 0.00242)$
7.13	Jet-switching phenomenon (vorticity contours). Notice how the wake first goes to the upward position, then goes to the downward position and then returns to the upward position. Also notice that the wake deflection angles are different for the upward and downward deflection. Flapping parameters: $Re = 1100$, $St = 0.9$, $h_a = 0.45$
7.14	Lift coefficient and drag coefficient time histories for the jet-switching wake. Flapping parameters: $Re = 1100$, $St = 0.9$, $h_a = 0.45$. Negative values of drag coefficient indicate thrust production
7 15	Contour map of propulsive efficiency vs. Strouhal number and heaving amplitude. 13'
	Contour map of thrust coefficient vs. Strouhal number and heaving amplitude 138
	Contour map of input power coefficient vs. Strouhal number and heaving amplitude. 138
	Pressure field during upstroke. Flapping parameters: $Re = 1100$, $St = 0.35$,
1.10	$h_a = 0.40, \ f = 0.4375 \ (k = 1.3744325).$ The sequence is from A (bottommost position) to H (topmost position), where: A) t = 13.725, B) t = 13.860, C) 14.0,
7.10	D) 14.168, E) 14.345, F) 14.476, G) 14.652, H) 14.828
7.19	Pressure coefficient distribution on the airfoil surface. Flapping parameters: $Re = 1100$, $St = 0.35$, $h_a = 0.40$, $f = 0.4375$ ($k = 1.3744325$). The sequence is from A (bottommost position) to D (topmost position). The pressure coefficient c_p was measured at the following instants: A) $t = 13.728$, B) $t = 14.124$, C) 14.476 , D) 14.828
7.20	Thrust coefficient distribution on the airfoil surface. Flapping parameters: $Re = 1100$, $St = 0.35$, $h_a = 0.40$, $f = 0.4375$ ($k = 1.3744325$). The sequence is from A (bottommost position) to D (topmost position). The thrust coefficient distribution $c_t(x/c)$ was measured at the following instants: A) $t = 13.728$, B) $t = 14.124$, C) 14.476 , D) 14.828
7.21	Pressure field during upstroke. Flapping parameters: $Re = 1100$, $St = 0.35$, $h_a = 0.15$, $f = 1.166667$ ($k = 3.665166$). The sequence is from A (bottommost position) to H (topmost position), where: A) $t = 5.120$, B) $t = 5.184$, C) 5.248, D) 5.317, E) 5.376, F) 5.456, G) 5.536, H) 5.6
7.22	Pressure coefficient distribution on airfoil surface. Flapping parameters: $Re = 1100$, $St = 0.35$, $h_a = 0.15$, $f = 1.166667$ ($k = 3.665166$). The sequence is from A (bottommost position) to D (topmost position). The pressure coefficient c_p was measured at the following instants: A) $t = 5.120$, B) $t = 5.280$, C) 5.456, D) 5.6 144
7.23	Thrust coefficient distribution on airfoil surface. Flapping parameters: $Re = 1100$, $St = 0.35$, $h_a = 0.15$, $f = 1.166667$ ($k = 3.665166$). The sequence is from A (bottommost position) to D (topmost position). The thrust coefficient distribution $c_t(x/c)$ was measured at the following instants: A) $t = 5.120$, B) $t = 5.280$, C)
	5.456, D) 5.6
7.24	Peak lift coefficient versus reduced frequency k . Flapping parameters: $Re = 1100$, $St = 0.35$

7.25	Top figure: time dependent thrust and lift coefficients (where negative values of drag coefficient indicate thrust production). Bottom figure: Heaving and pitching kinematics. Flapping parameters: $Re=1100, St=0.3, h_a=0.4, \alpha_a=20^{\circ}, \varphi=90^{\circ}$ ($\overline{c_t}=0.354186, \overline{c_l}=-0.001725$)
7.26	Average thrust coefficient and propulsive efficiency versus maximum pitching angle. Flapping parameters: $Re=1100,St=0.3,h_a=1.0.\ldots\ldots\ldots\ldots\ldots148$
7.27	Propulsive efficiency versus heaving amplitude. Flapping parameters: $Re=1100,$ $St=0.3.$
7.28	Average thrust coefficient versus heaving amplitude. Flapping parameters: $Re=1100,St=0.3.$
7.29	Average input power coefficient versus heaving amplitude. Flapping parameters: $Re=1100,St=0.3.$
7.30	Propulsive efficiency versus heaving amplitude for three different Strouhal number values. Flapping parameters: $Re=1100,\alpha_a=20.0.\ldots\ldots\ldots\ldots151$
7.31	Thrust coefficient versus heaving amplitude for three different Strouhal number values. Flapping parameters: $Re=1100,\alpha_a=20.0.\ldots\ldots\ldots\ldots152$
7.32	Input power coefficient versus heaving amplitude for three different Strouhal number values. Flapping parameters: $Re=1100,\alpha_a=20.0.\ldots\ldots\ldots\ldots152$
7.33	Propulsive efficiency and average thrust coefficient in function of the phase angle φ . Flapping parameters: $Re=1100, \alpha_a=30.0, h_a=0.5, St=0.25. \dots 153$
7.34	Comparison of the vorticity field for two different flapping cases during upstroke. Left column: flapping airfoil with a phase angle equal to $\varphi=100^\circ$. Right column: flapping airfoil with a phase angle equal to $\varphi=90^\circ$. Flapping parameters: $Re=1100,\ St=0.25,\ h_a=0.25,\ \alpha_a=10^\circ$. The sequence is shown for four instants during the upstroke motion, where: A) t = 8.0 B) t=8.35 C) t=8.70 D) t = 9.0 . 154
7.35	Contour map of propulsive efficiency vs. maximum pitching angle and heaving amplitude. Flapping parameters: $Re=1100,St=0.2$
7.36	Contour map of thrust coefficient vs. maximum pitching angle and heaving amplitude. Flapping parameters: $Re=1100,St=0.2.\ldots\ldots\ldots\ldots$ 156
7.37	Contour map of input power coefficient vs. maximum pitching angle and heaving amplitude. Flapping parameters: $Re=1100,St=0.2.\ldots\ldots\ldots\ldots156$
7.38	Contour map of propulsive efficiency vs. maximum pitching angle and heaving amplitude. Flapping parameters: $Re=1100,St=0.3\ldots\ldots\ldots\ldots$ 157
7.39	Contour map of thrust coefficient vs. maximum pitching angle and heaving amplitude. Flapping parameters: $Re=1100,St=0.3.$
7.40	Contour map of input power coefficient vs. maximum pitching angle and heaving amplitude. Flapping parameters: $Re=1100,St=0.3.\ldots\ldots\ldots\ldots158$
7.41	Contour map of propulsive efficiency vs. maximum pitching angle and heaving amplitude. Flapping parameters: $Re=1100,St=0.4$
7.42	Contour map of thrust coefficient vs. maximum pitching angle and heaving amplitude. Flapping parameters: $Re=1100,St=0.4,\ldots,\ldots,\ldots$. 159
7.43	Contour map of input power coefficient vs. maximum pitching angle and heaving amplitude. Flapping parameters: $Re = 1100$, $St = 0.4$.

First column: $Re=1100$, $St=0.2$, $h_a=1.0$, $\alpha_a=5^\circ$, $\varphi=90^\circ$. Second column: $Re=1100$, $St=0.2$, $h_a=1.0$, $\alpha_a=10^\circ$, $\varphi=90^\circ$. Third column: $Re=1100$, $St=0.2$, $h_a=1.0$, $\alpha_a=20^\circ$, $\varphi=90^\circ$. Fourth column: $Re=1100$, $St=0.2$, $h_a=1.0$, $\alpha_a=30^\circ$, $\varphi=90^\circ$. The sequence is shown for six instants during the upstroke motion, where: A) t = 30.0 B) t= 31.0 C) t= 32.0 D) t = 33.0 E) t =	160
Comparison of the vorticity field for four different flapping cases during upstroke. First column: $Re=1100,\ St=0.4,\ h_a=1.0,\ \alpha_a=5^\circ,\ \varphi=90^\circ.$ Second column: $Re=1100,\ St=0.4,\ h_a=1.0,\ \alpha_a=20^\circ,\ \varphi=90^\circ.$ Third column: $Re=1100,\ St=0.4,\ h_a=1.0,\ \alpha_a=30^\circ,\ \varphi=90^\circ.$ Fourth column: $Re=1100,\ St=0.4,\ h_a=1.0,\ \alpha_a=40^\circ,\ \varphi=90^\circ.$ The sequence is shown for six instants during the upstroke motion, where: A) t = 20.0 B) t= 20.5 C) t= 21.0 D) t= 21.5 E) t=	161
Heaving and flapping motions propulsive efficiency comparison. Flapping param-	
Heaving and flapping motions thrust coefficient comparison. Flapping parameters: $ \\$	
Heaving and flapping motions input power coefficient comparison. Flapping parameters: $Re=1100,\ St=0.3,\ \alpha_a=30.0.\ \dots$	163
	164
Vorticity field for the flexible airfoil study. The sequence is shown for eight instants during the downstroke motion, where: A) $t = 8.33 \text{ B}$) $t = 8.45 \text{ C}$) $t = 8.55 \text{ D}$) $t = 8.70 \text{ E}$) $t = 8.80 \text{ F}$) $t = 8.90 \text{ G}$) $t = 9.0 \text{ H}$) $t = 9.16$. Flapping parameters: $Re = 1100$, $h_{flex} = 0.3$, $h_a = 0.25$, $St = 0.3$	165
Vorticity field for the flexible airfoil study (rigid airfoil case). The sequence is shown for eight instants during the downstroke motion, where: A) $t=8.33~B$) $t=8.45~C$) $t=8.55~D$) $t=8.70~E$) $t=8.80~F$) $t=8.90~G$) $t=9.0~H$) $t=9.16$. Flapping	
Comparison of the vorticity field for two different airfoils. Left column: NACA 0012 airfoil. Right column: Selig S1223 airfoil. Flapping parameters: $Re = 1100$, $St = 0.4$, $h_a = 0.3$. The sequence is shown for four instants during the upstroke	
Comparison of the vorticity field for two different airfoils. Left column: NACA 2212 airfoil. Right column: NACA 4612. Flapping parameters: $Re=1100,St=0.4,h_a=0.3$. The sequence is shown for four instants during the upstroke motion,	
Three-dimensional computational domain layout in the xy plane	173
Typical grid system employed in the current three-dimensional study. A) Side	
Isosurfaces of ω -criterion at the beginning of the upstroke (t=7.0). Flapping	
Isosurfaces of Q-criterion at the beginning of the upstroke (t=7.0). Flapping parameters: $St = 0.5, h_a = 0.25, Re = 500.$	
	$Re=1100,\ St=0.2,\ h_a=1.0,\ \alpha_a=10^\circ,\ \varphi=90^\circ.\ Fourth column:\ Re=1100,\ St=0.2,\ h_a=1.0,\ \alpha_a=30^\circ,\ \varphi=90^\circ.\ The sequence is shown for six instants during the upstroke motion, where: A) t=30.0 B) t=31.0 C) t=32.0 D) t=33.0 E) t=34.0 F) t=35.0. Comparison of the vorticity field for four different flapping cases during upstroke for the vorticity field for four different flapping cases during upstroke comparison of the vorticity field for four different flapping cases during upstroke first column: Re=1100,\ St=0.4,\ h_a=1.0,\ \alpha_a=20^\circ,\ \varphi=90^\circ.\ Fourth column:\ Re=1100,\ St=0.4,\ h_a=1.0,\ \alpha_a=30^\circ.\ \varphi=90^\circ.\ Fourth column:\ Re=1100,\ St=0.4,\ h_a=1.0,\ \alpha_a=30.0.\ Flapping parameters:\ Re=1100,\ St=0.3,\ Ra=30.0.\ Flapping parameters:\ Re=1100,\ Ra=100,\ Ra$

8.6	Isosurfaces of λ_2 -criterion at the beginning of the upstroke (t=7.0). Flapping	
	7 6 7	. 178
8.7	Isosurfaces of N_k -criterion at the beginning of the upstroke (t=7.0). Flapping parameters: $St = 0.5, h_a = 0.25, Re = 500$. 179
8.8	Isosurfaces of pressure field at the beginning of the upstroke (t=7.0). Flapping	
	parameters: $St = 0.5, h_a = 0.25, Re = 500$	180
8.9	Spanwise vorticity contours at the beginning of the upstroke (t=7.0). Flapping parameters: $St = 0.5, h_a = 0.25, Re = 500$. A) Spanwise vorticity contours for the infinite-span wing (2D case). B) Rear view of the wing-tip vortices for the finite-span wing, where TVL is the left wing-tip vortex and TVR is the right wing tip vortex. C) Spanwise vorticity contours for the finite-span wing at the symmetry plane (3D case). D) Spanwise vorticity contours for the finite-span wing in the plane located at a distance equal to $d = 0.4 \times c$ measured from the wing symmetry plane (3D case)	. 184
8.10	Vortex topology at the beginning of the upstroke (t=7.0). Flapping parameters: $St = 0.5, h_a = 0.25, Re = 500$. A) Side view. B) Perspective view	
8.11	Vortex topology at the beginning of the upstroke (t=7.0). Flapping parameters: $St = 0.5, h_a = 0.25, Re = 500$. A) Side view. B) Top view	
8.12	Vortex topology at the beginning of the upstroke (t=7.0). Flapping parameters: $St = 0.15, h_a = 0.075, Re = 500$. A) Side view. B) Perspective view	
8.13	Vortex topology at the beginning of the upstroke (t=7.0). Flapping parameters: $St = 0.15, h_a = 0.075, Re = 500$. A) Side view. B) Top view	. 188
8.14	Vortex topology during downstroke (t=6.75). Flapping parameters: $St = 0.5, h_a = 0.25, \alpha_a = 10^{\circ}, Re = 500$. A) Side view. B) Top view. C) Perspective view	
	Vortex topology during downstroke (t=6.75). Flapping parameters: $St=0.5, h_a=0.25, \alpha_a=20^\circ, Re=500.$ A) Side view. B) Top View. C) Perspective view	
8.16	Streamlines visualization during downstroke (t=6.75). Flapping parameters: $St = 0.5, h_a = 0.25, \alpha_a = 10^{\circ}, Re = 500$. A) Front view. B) Top View. C) Perspective view. D) Perspective view.	100
8.17	view. D) Perspective view	193
8.18	Different wing platforms used for the study of aspect ratio influence on the aero-dynamic performance.	
8.19	Vortex topology for the rolling wing case (t=5.0). Flapping parameters: $St = 0.10, f_{roll} = 1.0, Re = 500$. A) Perspective view. B) Top view. In this view the	101
8.20	right wing-tip corresponds to the hinged extreme. C) Side view Vortex topology for the rolling wing case (t=5.0). Flapping parameters: $St =$	196
	$0.25, f_{roll} = 1.0, Re = 500$. A) Perspective view. B) Top view. In this view the right wing-tip corresponds to the hinged extreme. C) Side view	. 197
8.21	Vortex topology for the rolling wing case (t=5.0). Flapping parameters: $St=0.38, f_{roll}=1.0, Re=500.$ A) Perspective view. B) Top view. In this view the	
8.22	right wing-tip corresponds to the hinged extreme. C) Side view Streamlines visualization during downstroke (top view), the streamlines are colored according to the velocity magnitude values. In this view the right wing-tip corresponds to the hinged extreme. Flapping parameters: $St = 0.38$, $f_{roll} = 1.0$, $Re = 1.0$	198
	500. A) t=5.0 B) t=5.05 C) t=5.10 D) t=5.15	199

List of Tables

$4.1 \\ 4.2$	Some of the currently used grid generation methods
4.2	systems
6.1	Maximum error at $t=1.0$ and $\nu=0.1$ for a trigonometric analytic solution ($\omega_0=\omega_1=\omega_3=1$). The estimated convergence rate p is also shown. The column entitled as h_1/h_g denotes the ratio of the grid spacing on grid 1 to the spacing on
	grid g
6.2	Drag coefficient (c_d) and length of wake bubble (L) for $Re=20$ and $Re=40$ 9
6.3	Drag coefficient (c_d) and lift coefficient (c_l) for $Re = 100$ and $Re = 200$ 9
6.4	Summary of the overlapping grid system used for the cases where $Re = 20$, $Re = 100$
	$40, Re = 100 \text{ and } Re = 200. \dots 900. \dots 9000. \dots 9000000000000000000$
6.5	Summary of the overlapping grid system used for the benchmarking computations. 99
6.6	Comparison of the performance of different direct and iterative solvers
6.7 6.8	Comparison of c_d and c_l coefficients for both cases at $t = 7.0.$
6.9	Kinematics parameters for the pitching airfoil case
0.9	pitching airfoil case
6 10	Kinematics parameters for the heaving-and-pitching airfoil case
	Average thrust coefficient $\overline{c_t}$ and maximum lift coefficient $\widehat{c_l}$ comparison for the
0.11	heaving-and-pitching airfoil case
6.12	Average thrust coefficient $\overline{c_t}$ comparison between the present results and the results
	obtained by Wang [207]
6.13	Comparison of average thrust coefficient $\overline{c_t}$
6.14	Comparison of average thrust coefficient $\overline{c_t}$
6.15	Parallel computations benchmarking results
	Description of grids used for the grid refinement study (for force measurements) 115
6.17	Observed values of the average thrust coefficient $\overline{c_t}$ for each grid. The observed
	order of convergence and the equivalent zero grid spacing values are also shown $11'$
	Comparison of the performance of different direct and iterative solvers
	Description of grids used for the grid refinement study (wake structures resolution). 12
	Description of grids used for the grid refinement study
6.21	Computational resources used in each benchmarking case
7.1 7.2	Flapping parameters for the pure heaving case
	$St = 0.3, h_a = 1.0. \dots 148$

7.3	Flapping parameters for the study of the effect of heaving amplitude h_a on the aerodynamic performance	149
7.4	Flapping parameters for the study of the effect of Strouhal number St on the aerodynamic performance	
7.5	Flapping parameters for the study of the effect of phase angle φ on the aerodynamic performance.	
7.6	Flapping parameters for the study of the flexible heaving airfoil	
7.7	Airfoils used for the study of cambering effect on the aerodynamic performance of heaving airfoils	167
7.8	Heaving parameters for the study of airfoil cambering effect on the aerodynamic performance.	167
7.9	Comparison of the aerodynamic performance of eight different airfoils for the study of cambering effect on the aerodynamic behavior. Flapping parameters: $Re =$	
7.10	1100, $St = 0.4$, $h_a = 0.1$, $f_h = 2.0$	167
	1100, $St = 0.4$, $h_a = 0.3$, $f_h = 2.0 \dots \dots$	167
8.1	Kinematics parameters for the pure heaving wing case	182
8.2	Simulation results for the pure heaving wing case (positive $\overline{c_t}$ values indicate thrust production whereas negative $\overline{c_t}$ values indicate drag production)	
8.2 8.3	production whereas negative $\overline{c_t}$ values indicate drag production) Simulation results for the pure heaving wing case. Comparison of the $3\mathbb{D}$ results versus the $2\mathbb{D}$ results (positive $\overline{c_t}$ values indicate thrust production whereas negative $\overline{c_t}$ values indicate drag production)	182 183
8.2 8.3 8.4	production whereas negative $\overline{c_t}$ values indicate drag production) Simulation results for the pure heaving wing case. Comparison of the $3\mathbb{D}$ results versus the $2\mathbb{D}$ results (positive $\overline{c_t}$ values indicate thrust production whereas negative $\overline{c_t}$ values indicate drag production)	182 183 184
8.2 8.3 8.4 8.5	production whereas negative $\overline{c_t}$ values indicate drag production)	182 183 184
8.2 8.3 8.4	production whereas negative $\overline{c_t}$ values indicate drag production) Simulation results for the pure heaving wing case. Comparison of the $3\mathbb{D}$ results versus the $2\mathbb{D}$ results (positive $\overline{c_t}$ values indicate thrust production whereas negative $\overline{c_t}$ values indicate drag production)	182 183 184 189
8.2 8.3 8.4 8.5 8.6	production whereas negative $\overline{c_t}$ values indicate drag production)	182 183 184 189
8.2 8.3 8.4 8.5	production whereas negative $\overline{c_t}$ values indicate drag production) Simulation results for the pure heaving wing case. Comparison of the $3\mathbb{D}$ results versus the $2\mathbb{D}$ results (positive $\overline{c_t}$ values indicate thrust production whereas negative $\overline{c_t}$ values indicate drag production)	182 183 184 189
8.2 8.3 8.4 8.5 8.6	production whereas negative $\overline{c_t}$ values indicate drag production) Simulation results for the pure heaving wing case. Comparison of the $3\mathbb{D}$ results versus the $2\mathbb{D}$ results (positive $\overline{c_t}$ values indicate thrust production whereas negative $\overline{c_t}$ values indicate drag production)	182 183 184 189 189
8.2 8.3 8.4 8.5 8.6	production whereas negative $\overline{c_t}$ values indicate drag production) Simulation results for the pure heaving wing case. Comparison of the $3\mathbb{D}$ results versus the $2\mathbb{D}$ results (positive $\overline{c_t}$ values indicate thrust production whereas negative $\overline{c_t}$ values indicate drag production)	182 183 184 189 189
8.2 8.3 8.4 8.5 8.6 8.7	production whereas negative $\overline{c_t}$ values indicate drag production) Simulation results for the pure heaving wing case. Comparison of the $3\mathbb{D}$ results versus the $2\mathbb{D}$ results (positive $\overline{c_t}$ values indicate thrust production whereas negative $\overline{c_t}$ values indicate drag production)	182 183 184 189 189

Acknowledgements

Financial support of the Marie Curie actions EST project FLUBIO, through grant MEST-CT-2005-020228 is acknowledged.

I would like to specially thank my thesis advisor Prof. Alessandro Bottaro, for giving me the opportunity to conduct my doctoral studies at the University of Genova and for supervising my research work and for constantly keeping me busy with new challenging and interesting subjects.

I wish to express my sincere gratitude to all the people I met during these last three years, who in one or another way influenced on my decisions and helped me during this period. Just to name a few: Joao, Ana, Bart, Giovanni, Andreas, Damian, Julien, Houssam, Hakan, Laura, Thomas, Bill, Dominic, Anna, Antoine, Marco, Simona, Valeria, Stephano, Gaby, Ernesto, Max, Sam, Laly (and I am deeply sorry for those I do not remember at the moment).

My successes are largely due to the quiet support of my family. I thank my parents for supporting the choices that I have made in my life, I also thank my brother and sister for always being there. Finally, I cannot pass this page without thanking the universal architect.

E Pluribus Unum

Abstract

The aim of this dissertation is to contribute to a better comprehension of the mechanism of flapping airfoils/wings propulsion and the associated unsteady aerodynamics, independently of their possible practical applications. We describe an accurate and stable numerical method to numerically solve the incompressible Navier-Stokes equations, which, used together with the overlapping grids method and to the numerical tools implemented, constitutes a very powerful tool to solve fluid dynamics problems with fixed and moving/deforming boundaries in two and three space dimensions. The two-dimensional results are presented for airfoils undergoing heaving and coupled heaving-and-pitching motion. The interest here is to determine the values of flapping frequency and flapping amplitude best suited for flapping flight, in terms of maximum propulsive efficiency and thrust production. We also study the influence of airfoil cambering and airfoil flexibility on the aerodynamic performance. Finally, three-dimensional rigid finite-span wings undergoing heaving, coupled heaving-and-pitching and root-flapping motion modes are investigated, with focus on the wake topology and aerodynamic performance, and their dependence on the flapping motion parameters. We also establish the best criteria for vortical structures identification and assess whether the assumption of two-dimensionality has some validity in three-dimensional cases.